

## Classification on Herman Rings of Extended Blaschke Equations

David C. Ni

Direxion Technology, 9F, 177-1 Ho-Ping East Road Section 1,  
Taipei, Taiwan, R.O.C.

Chou Hsin Chin

Department of Electro-Physics, National  
Chiao Tung University, Hsin Chu, Taiwan, R.O.C.

**Abstract.** This paper presents some interesting results of numerical analysis of the Extended Blaschke functions, which are constructed by extending Blaschke product. On the complex plane, the convergent domains of the functions form fractal patterns of constrained Herman rings with limited-layered structures, which demonstrate skip-symmetry, symmetry broken, chaos, and degeneracy in conjunction with parameter space.

### 1. Introduction

The family  $\{F_n\}$  of complex analytic functions defined on an open set  $U$  is a normal family if every infinite sequence of maps from  $\{F_n\}$  has a subsequence, which converges uniformly on compact subsets of  $U$ , or converges uniformly to  $\infty$  on  $U$ . The Fatou set,  $F(f)$ , on the Riemann sphere is the largest open set such that the iterates  $\{f^n \mid F: n \geq 1\}$  form a normal family. The Julia set,  $J(f)$ , is the complement of the Fatou set. In this paper, we adopt the definition of absolute and bounded convergence since the iteration on computer is finite.

Herman rings represent a class in meromorphic dynamical systems [1, 2]. A periodic component  $U$  of Fatou set, with  $f^n(U) = U$ , is an annulus and  $f^n$  acts on  $U$  as an irrational rotation,  $U$  is then classified as a Herman ring. Herman used Arnold's theorem about real analytical conjugations of real analytic diffeomorphism of circle to rigid rotations when the rotation number is like a Siegel number [3]. Herman indicated that the map  $z \rightarrow \exp(i\theta)z^{-1}[(a-z)/(1-\bar{a}z)]^2$  includes such regions with appropriate values of  $\theta$  and  $a$  [4].

In our previous efforts we extended this map by studying  $h(z) = \prod_4 \{ \exp(g_i(z)) [(a_i - z)/(1 - \bar{a}_i z)] \}$ , which have been further generalized and defined hereby as extended Blaschke products [5]. This set of products reveals some interesting characteristics. We have also adopted our studies for the applications in the antenna areas [6, 7] and elaborated the mathematical foundation [8]. In addition, we have discussed the special hierarchical structures of Herman rings and their chaotic behavior [9, 10].

In this paper we classify this class of functions and equations in the form of iterated maps by means of numerical analysis. We present a set of special features, such as limited number of high-degree Herman rings,

skip-symmetry, symmetry broken, chaos, and degeneracy of the rings in conjunction with the parameter space of the functions and equations.

## 2. Function Construction and Class Formation

### 2.1 Functions and Equations

We define the set of functions  $f = z^q \prod C_i$ , where  $z$  is a complex variable,  $q$  is a rational number, and  $C_i$  has the following form:

$$C_i = \exp(g_i(z))[(a_i - z)/(1 - \bar{a}_i z)] \tag{1}$$

Here  $\bar{a}_i$  is the complex conjugate of a complex number  $a_i$ . The function  $f$  defined hereby can be viewed as extended Blaschke products. The degree of  $f(z) = P(z)/Q(z)$  is defined as  $\text{Max}\{\text{deg } P, \text{deg } Q\}$ . This function explicitly includes the formulas of three important theories in physics. The first one concerns the special relativity theory by A. Einstein:

$$u_x' = (u_x - v) / (1 - vu_x/c^2) \tag{2}$$

The term  $z^q$  is related to the potential energy of Newtonian mechanics. In this paper we focus on  $q = -1$  case. We also illustrate the cases of  $q = -0.5$  and  $q = -1.5$  for discussing fractal and chaos comparing with the  $q = -1$  case. The term  $\exp(g_i(z))$  represents the phase parameter which has the form of a solution of Maxwell's equations for electromagnetism. The term  $g_i(z)$  is a complex function and is assigned by  $\sum_n 2\pi i n z$ .

The extended Blaschke equation is defined as follows:

$$f(z) - z = z^q \prod C_i - z = 0 \tag{3}$$

### 2.2 Parameter Space

To characterize the original and the mapped domains, we define a set of parameters called parameter space. The parameter space includes six parameters: (1)  $z$ , (2)  $a$ , (3)  $\exp(g_i(z))$ , (4)  $q$ , (5) *iteration*, and (6) *degree*. In the context of the paper we use  $\{z, a, \exp(g_i(z)), q, \textit{iteration}, \textit{degree}\}$  to represent this parameter space. For example,  $\{a\}$ , is one of the subsets of the parameter space.

### 2.3 Original and Mapped Domains

A domain can be the entire complex plane,  $C_\infty$ , or a set of complex numbers, such as  $z = x + yi$ , with  $(x^2 + y^2)^{1/2} \leq R$ , and  $R$  is a real number. For solving the extended Blaschke equations a function  $f$  will go through iteration as:

$$f^n(z) = f \circ f^{n-1}(z), \tag{4}$$

Where  $n$  is a positive integer indicating the number of iteration. The function operates on a domain called original domain and the set of  $f^n(z)$  is mapped domain. In the figures, the regions in black color represent Fatou sets, and the blank (white) regions correspond to Julia sets. In the paper we discuss the following functions:

- (1)  $Z^{-1} C$  – second degree of the functions
- (2)  $Z^{-1} C_1 C_2$  – third degree the functions
- (3)  $Z^{-1} C_1 C_2 C_3$  – fourth degree of the functions
- (4)  $Z^{-1} C_1 C_2 C_3 C_4$  – fifth degree of the functions.

(5) degrees higher fifth degree are shown as complementary examples

### 2.4 Constrained Herman Rings

As defined in Section 1, we have examined the Fatou components that are conformally isomorphic to an annulus and the action of some  $f^n$  is conjugate to irrational rotation. Figure 1(a) and 1(b) show the original and the mapped domains of  $f^n$  of 11<sup>th</sup> degree respectively. Both domains are at scale of  $10^{10}$ . The rings at larger and smaller scales are not shown. Due to the complexity of multiple-layered rings we are not able to verify the existence of an irrational rotation as defined for Herman rings. We therefore adopt the term of constrained Herman rings for these sets.

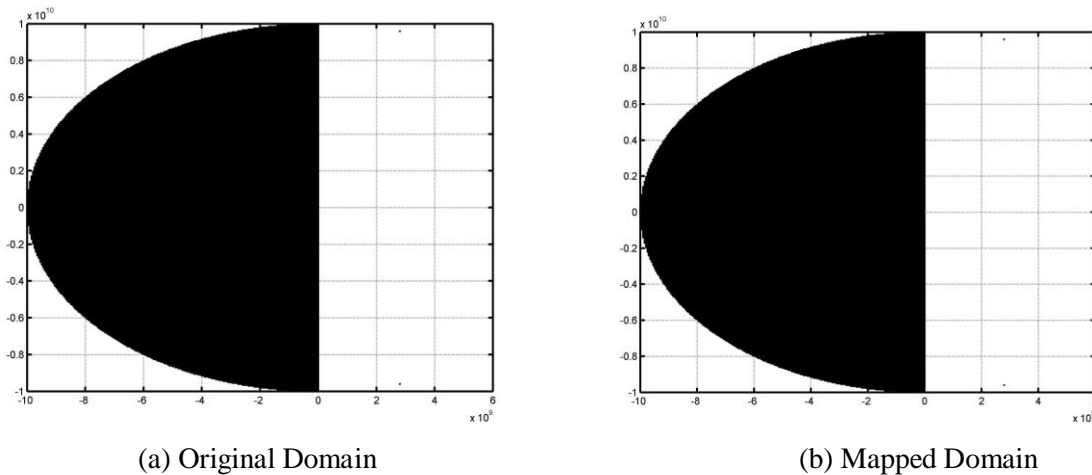


Fig. 1 (a) Original Domain and (b) Mapped domain of  $Z^{-1} C^{10}$ .

## 3. Classification

### 3.1 Herman Rings of Original Domains

We classify the original domains of functions:  $Z^{-1} C$ ,  $Z^{-1} C_1 C_2$ ,  $Z^{-1} C_1 C_2 C_3$ , and  $Z^{-1} C_1 C_2 C_3 C_4$  with some extension to the functions of higher degrees.

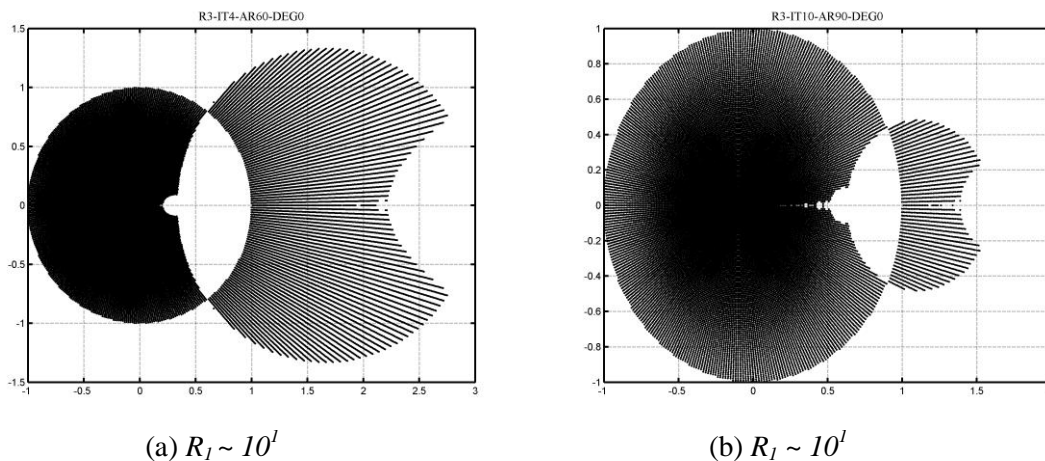


Fig. 2 Original Domains of function  $Z^{-1} C$ .

Figure 2 shows the original domains of the function  $Z^{-1} C$ . Figure 2 (a) and (b) show that Fatou and Julia sets form a group of 2-layer constrained Herman rings in conjunction with parameter subset  $\{a, iteration\}$ . These 2-layer domains are in the range of  $R_l \sim 10^l$  scale. Beyond of scale of  $10^l$ , we have not observed any other existing Fatou sets. Fig 2(a) and (b) show fractal patterns for two different values of the parameter  $\{a\}$ .

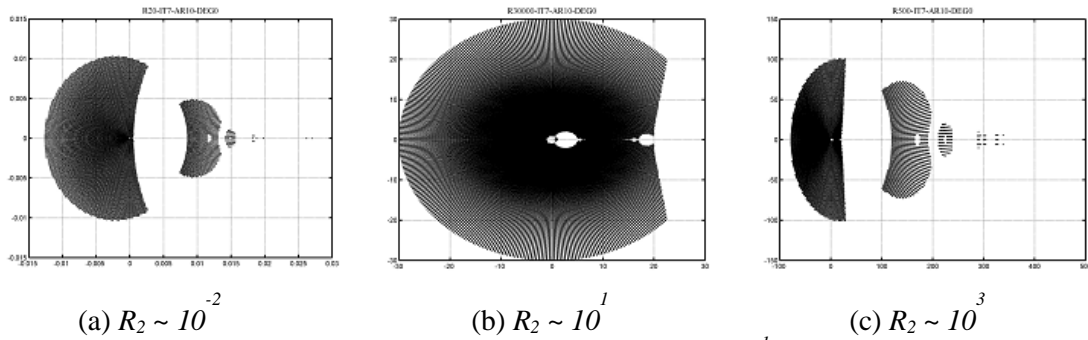


Fig. 3 Original Domains of function of  $Z^{-1} C_1 C_2$

Figure 3 shows the original domains of the function  $Z^{-1} C_1 C_2$ . Figure 3 (a), (b) and (c) show that Fatou and Julia sets form a group of 3-layer constrained Herman rings in conjunction with the parameter subset  $\{a, iteration\}$ . Figure 3(a) shows several disconnected Fatou sets at scale of  $R_2 \sim 10^{-2}$ . Figure 3(b) shows several Fatou and Julia sets at scale of  $R_2 \sim 10^1$ . The sets in Figure 3(a) are around the point  $z = 0$  at Figure 3(b). Figure 3(c) shows several disconnected Fatou sets at scale of  $R_2 \sim 10^3$ . Figure 3(b) is actually the leftmost set on the Figure 3(c).

Figure 4 shows the original domains of the function  $Z^{-1} C_1 C_2 C_3$ . Figure 4 (a), (b), (c), (d), and (e) show that the Fatou and Julia sets form a group of 5-layer partial Herman-Ring fractal domains in conjunction with parameter subset  $\{a, iteration\}$ .

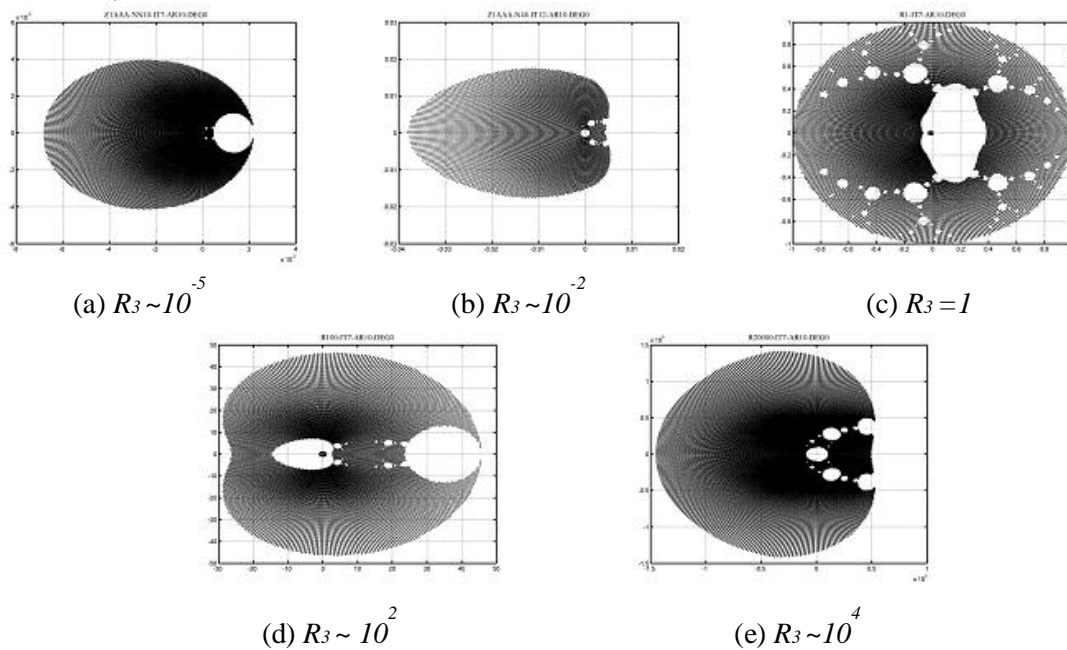


Fig. 4 Original Domains of function of the form  $Z^{-1} C_1 C_2 C_3$ .

Figure 4(a) shows a constrained Herman ring at scale of  $10^{-5}$ . Figure 4(b) shows a constrained Herman ring at scale of  $R_3 \sim 10^{-2}$ . Figure 4(c) shows a constrained Herman ring at scale of  $R_3 = 1$ . The sets in Figure 4(b) can be seen locating around  $z = 0$  in Figure 4(c). Figure 4(d) shows a constrained Herman-Ring at scale of  $R_3 \sim 10^2$ . Figure 4(c) can be seen locating around  $z = 0$  at Figure 4(d). Figure 4(e) shows a constrained Herman ring at scale of  $R_3 \sim 10^4$ . Figure 4(d) is locating around  $z = 0$  at Figure 4(e). We have explored possibly existing Fatou sets beyond the scales of 4(a) and 4(e), namely,  $R_3 < 10^{-5}$  and  $R_3 > 10^4$  as in the cases of the functions of  $Z^{-1} C$  and  $Z^{-1} C_1 C_2$ . For the lower bound beyond  $R_3 \sim 10^{-5}$ , the result is straightforward since there are no blank regions (the Julia sets) existing for forming Herman rings at smaller scales around  $z = 0$ . For the upper bound we have elaborated up to  $10^{100}$  range and could not find any existing Fatou sets (black regions). We have hereby observed only five layers of constrained Herman rings for this function.

Figure 5 shows the original domains of the function  $Z^{-1}C_1C_2C_3C_4$ . Figure 5 (a), (b), (c), (d) and (e) show that the Fatou and Julia sets also form a group of 5-layer constrained Herman rings in conjunction with parameter subset  $\{a, iteration\}$ . Figure 5(a) shows a constrained Herman ring at scale of  $R_4 \sim 10^{-6}$ . Figure 5(b) shows a constrained Herman ring at scale of  $R_4 \sim 10^{-2}$ . Figure 5(c) shows a constrained Herman ring at scale of  $R_4 = 1$ . The sets in Figure 5(b) can be seen locating around  $z = 0$  point at Figure 5(c). Figure 5(d) shows a constrained Herman ring at scale of  $R_4 \sim 10^2$ . Figure 5(c) can be seen locating around  $z = 0$  point at Figure 5(d). Figure 5(e) shows a constrained Herman ring at scale of  $R_4 \sim 10^6$ . Figure 5(d) is locating around  $z = 0$  at Figure 5(e). The constrained Herman ring at scale of  $10^{-6}$  is topologically similar to that at scale of  $10^2$  and the Herman ring at scale of  $10^{-2}$  is topologically similar to that at  $10^6$ . This portrait is similar to the Herman rings for both  $Z^{-1}C_1C_2$  and  $Z^{-1}C_1C_2C_3$  functions. We call the symmetry that a skip-layer symmetry. This symmetry is important to understand the mapping between original and mapped domains.

We have explored several functions with degrees higher than the 5<sup>th</sup>-degree and found that the number of layers keeps the same as for  $Z^{-1}C_1C_2C_3$ , namely, only 5 layers constrained Herman rings are observed at 12<sup>th</sup> degree as an example. The skip-layer symmetry is also observed in the higher-degree sets.

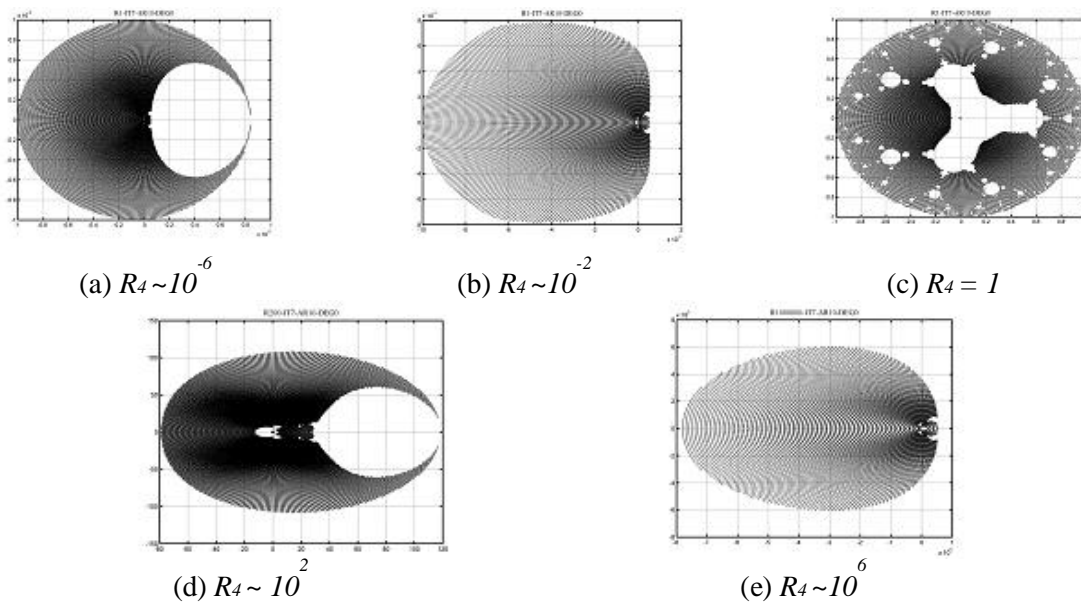
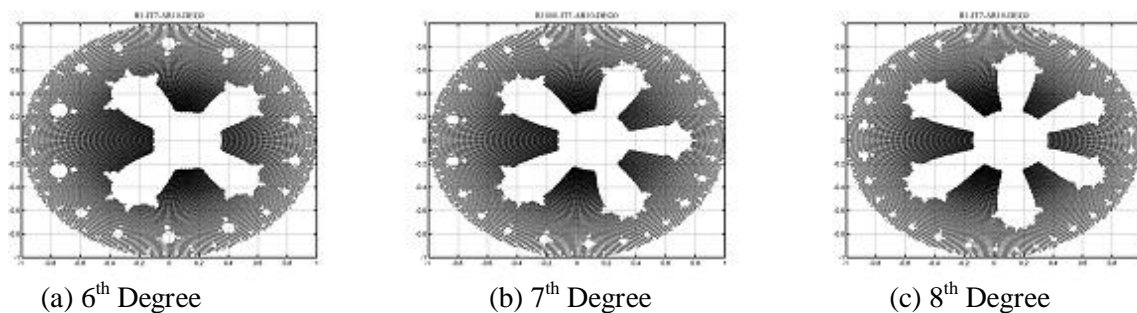


Fig. 5 Original Domains of the functions of the form  $Z^{-1}C_1C_2C_3C_4$

Figure 6 shows the constrained Herman rings at  $R = 1$  scale for different function degrees. The number of branches of the central portion of the fractals is two less than the functional degree. For example, the 7<sup>th</sup>-degree domain has 5 branches, and each branch extends into 5 bulbs. The individual bulb further extends into 5 second-level bulbs on the 2<sup>nd</sup> layer and so on. The high-level bulbs will further close to the boundary of unit circle with radius = 1.



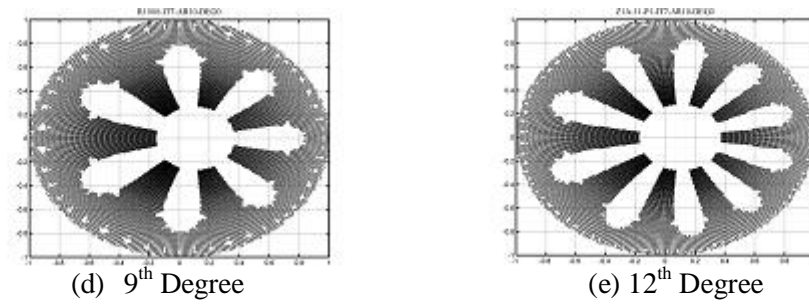


Fig. 6 Herman Rings for different function degrees for  $R = 1$  scale.

Table 1 shows the layers and corresponding scales of the sets for different function degrees.

$Z^{-1} \prod_i C_i$	$d = 2$	$d = 3$	$d = 4$	$d = 5$	$d = 6$	$d = 7$	$d = 8$	$d = 9$
Layers	2	3	5	5	5	5	5	5
Scale 1	$10^1$	$10^{-2}$	$10^{-5}$	$10^{-6}$	$10^{-7}$	$10^{-9}$	$10^{-10}$	$10^{-11}$
Scale 2	$10^1$	$10^1$	$10^{-2}$	$10^{-2}$	$10^{-2}$	$10^{-3}$	$10^{-4}$	$10^{-5}$
Scale 3		$10^3$	1	1	1	1	1	1
Scale 4			$10^2$	$10^2$	$10^3$	$10^3$	$10^3$	$10^4$
Scale 5			$10^4$	$10^6$	$10^7$	$10^9$	$10^9$	$10^{11}$

Table 1 Scales of Fatou Sets for different degrees ( $d$ ) for a particular parameter  $\{a\}$

### 3.2 Mapped Domains

There are several scenarios to examine the mapped domains. We have chosen the following three scenarios:

1. The mapped domains of the Fatou sets in the original domains.
2. The mapped domains of a special set of the original domain. This set includes both Fatou and Julia sets. For example, a circle on complex plane with  $radius = 0.5$ .
3. The trace of each step of the iteration of a specific point in a Fatou or a Julia set.

Fig. 7 shows the mapped domain of the original domain of the function  $Z^{-1} C_1 C_2 C_3$  (Fig. 4(c)) with  $R_3 = 1$ . This mapped domain is obtained through 20 iteration and with points distributed within circle with  $radius = 1$  on the complex plane. Further examining on this mapped domain, we find that the point set in the region defined by  $(x^2 + y^2)^{1/2} < 1$  is symmetrical to the real axis,  $y = 0$ ; while the point set on  $(x^2 + y^2)^{1/2} = 1$  is randomly distributed. We will discuss this observation in the next section.

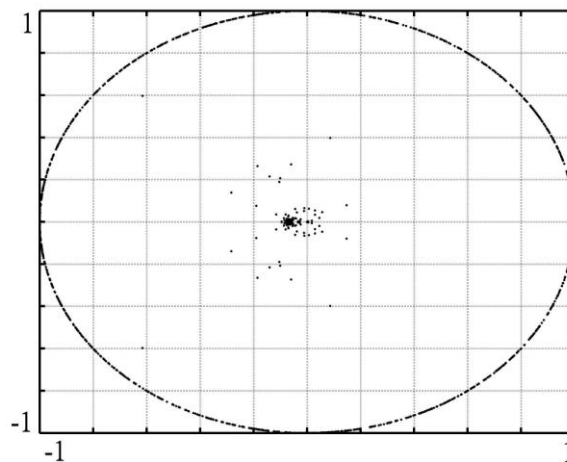


Fig. 7 A mapped domain of a original convergent domain (Fatou sets) of the function  $Z^{-1} C_1 C_2 C_3$  (Fig. 4(c)) with scale of  $R = 1$ .

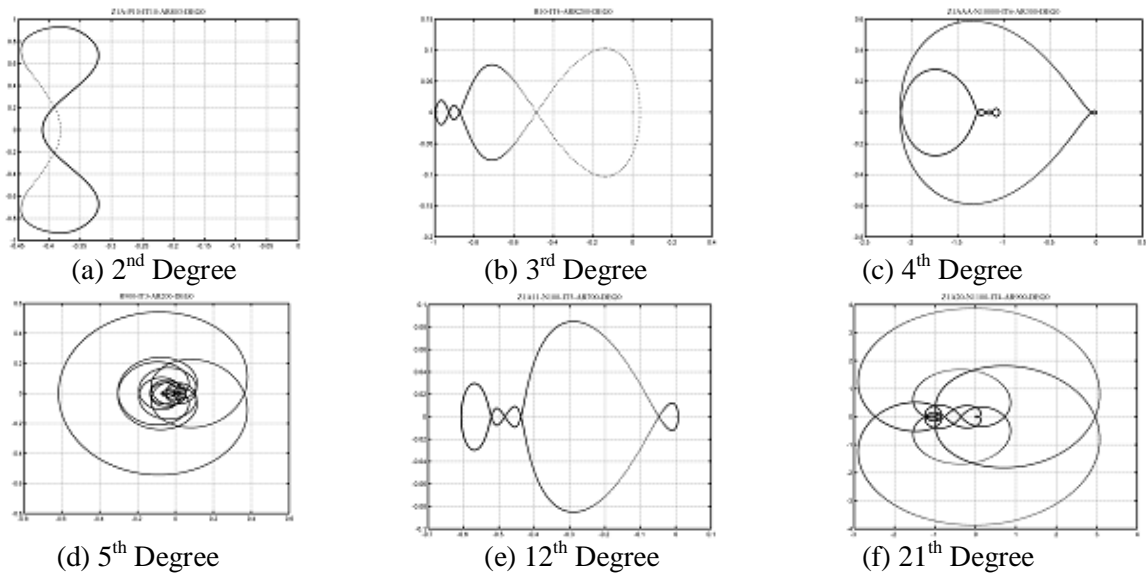


Figure 8 Mapped domains for different degrees.

For the second scenario, we define a circle on the complex plane as an original domain and compute the mapped domain. Figure 8 shows some mapped domains for different function degrees. From geometrical perspective, the algebraic curves in Fig. 8(a) and 8(b) can be the trajectories on torus with  $genus = 1$ , while the ones of 3<sup>rd</sup> degree or higher can not be projections of trajectories on torus with  $genus = 1$ .

For the third scenario, we select a point in the original domain and compute the trajectories generated by iteration. We select points on the original domain of the function  $Z^{-1} C_1 C_2 C_3$ .

Fig. 9 shows the trajectories. The start point is marked by a square symbol and the end point is marked by a diamond symbol. Fig. 9(a) shows a point on the circle with  $radius = 1$  that converges to another point and Fig. 9(b) shows a fast convergent point inside the circle with  $radius = 1$ . All the points on an original convergent domain will be mapped to a set of points which are subjected to the precision of computer platform. Periodic solutions corresponding to iteration steps are observed.

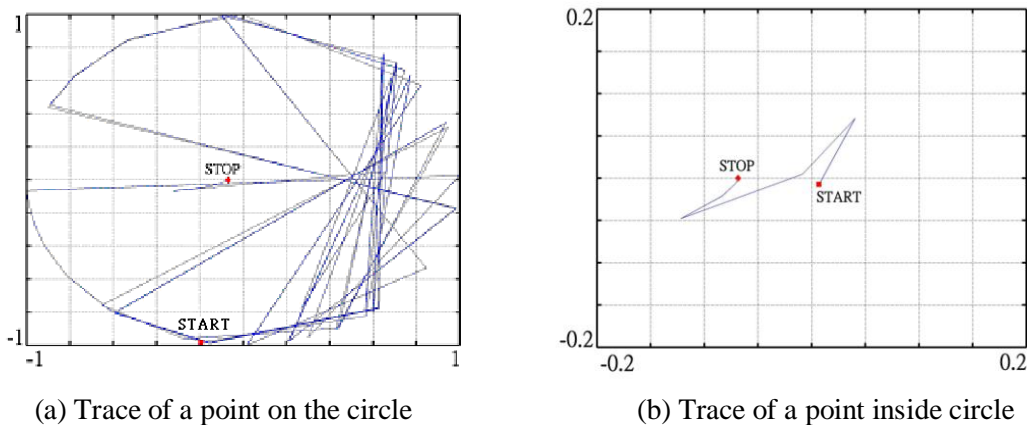


Figure 9 Traces of points generated by a given number of iteration (a) point on a circle with  $radius = 1$  (b) point inside a circle with  $radius = 1$ . The trace starts from the point marked by square symbol and stops at the point marked by diamond symbol.

#### 4. Symmetry Broken and Chaos

From geometrical perspective, we have observed that both original and mapped domains are symmetrical to the

real axis. This symmetry can be influenced by the parameters which can transform a stable domain (Herman ring with stable Fatou and Julia sets) to a chaotic domain (disconnected Fatou and Julia sets). A chaotic domain shows random patterns of Fatou sets after consecutive iterations and eventually Fatou sets disappear, namely, the domain will become a Julia set or connected Julia sets only, and Herman rings do not exist anymore. However, the proper selections of the parameters can prevent stable domains from evolving to chaotic ones.

#### 4.1 Symmetry Broken in Original and Mapped Domains

Fig. 10 shows four original domains, including Fatou and Julia sets, of the function  $Z^{-1}C_1C_2C_3$  with different values of parameter  $\{a\}$ . Fig. 10(a) is with  $a = 0.01$ , Fig. 10(b) is with  $a = 0.1$ , Fig. 10(c) is with  $a = 0.2$ , and 10(d) is with  $a = 1$ .

As the value of the parameter  $\{a\}$  increases, the Julia sets in the Herman rings become asymmetric to the imaginary axis. When  $a = 1$ , the original domain becomes chaotic, namely, disconnected and randomized Fatou and Julia sets.

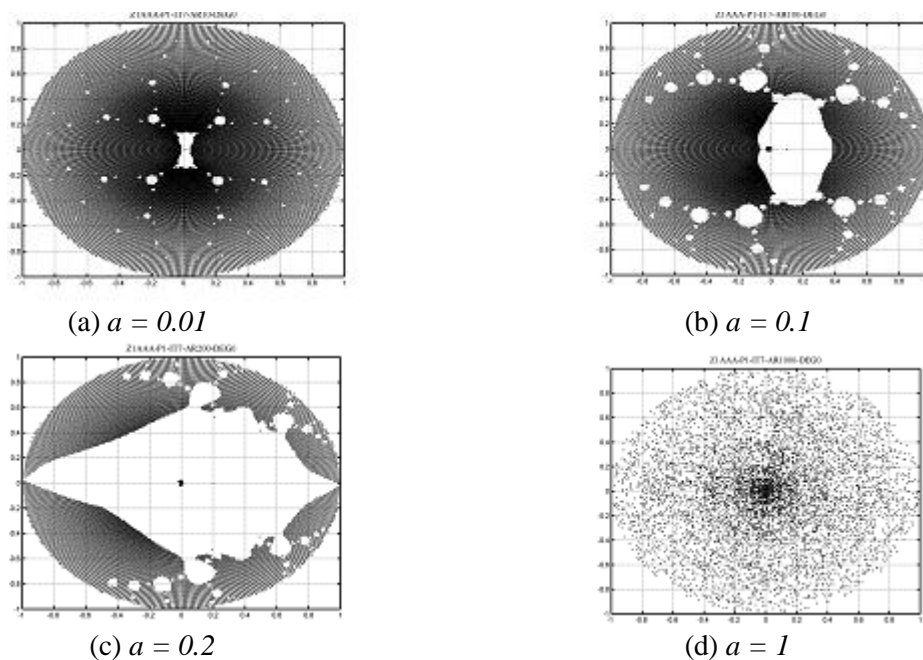


Figure 10 The original domains with different values of parameter  $\{a\}$ .  
 (a)  $a = 0.01$  (b)  $a = 0.1$  (c)  $a = 0.2$  and (d)  $a = 1$

For the mapped domain as shown in Fig. 7 we can divide the original domain with  $radius = 1$  of the function  $Z^{-1}C_1C_2C_3$  into two regions: one region includes all point with  $(x^2 + y^2)^{1/2} < 1$  and the other includes the points on the perimeter of the region, namely,  $(x^2 + y^2)^{1/2} = 1$ . Figure 11 shows mapped domain obtained from the original domain defined by  $(x^2 + y^2)^{1/2} \leq 0.99$  that form a set of points which are symmetrical to the real axis. As the iteration number increases to a threshold value of computer accuracy, we observe that a set of periodic points are still symmetrical to the real axis (as shown in Fig. 11(a) through 11(c) with different iteration numbers). This set includes the solutions of the extended Blaschke equations.

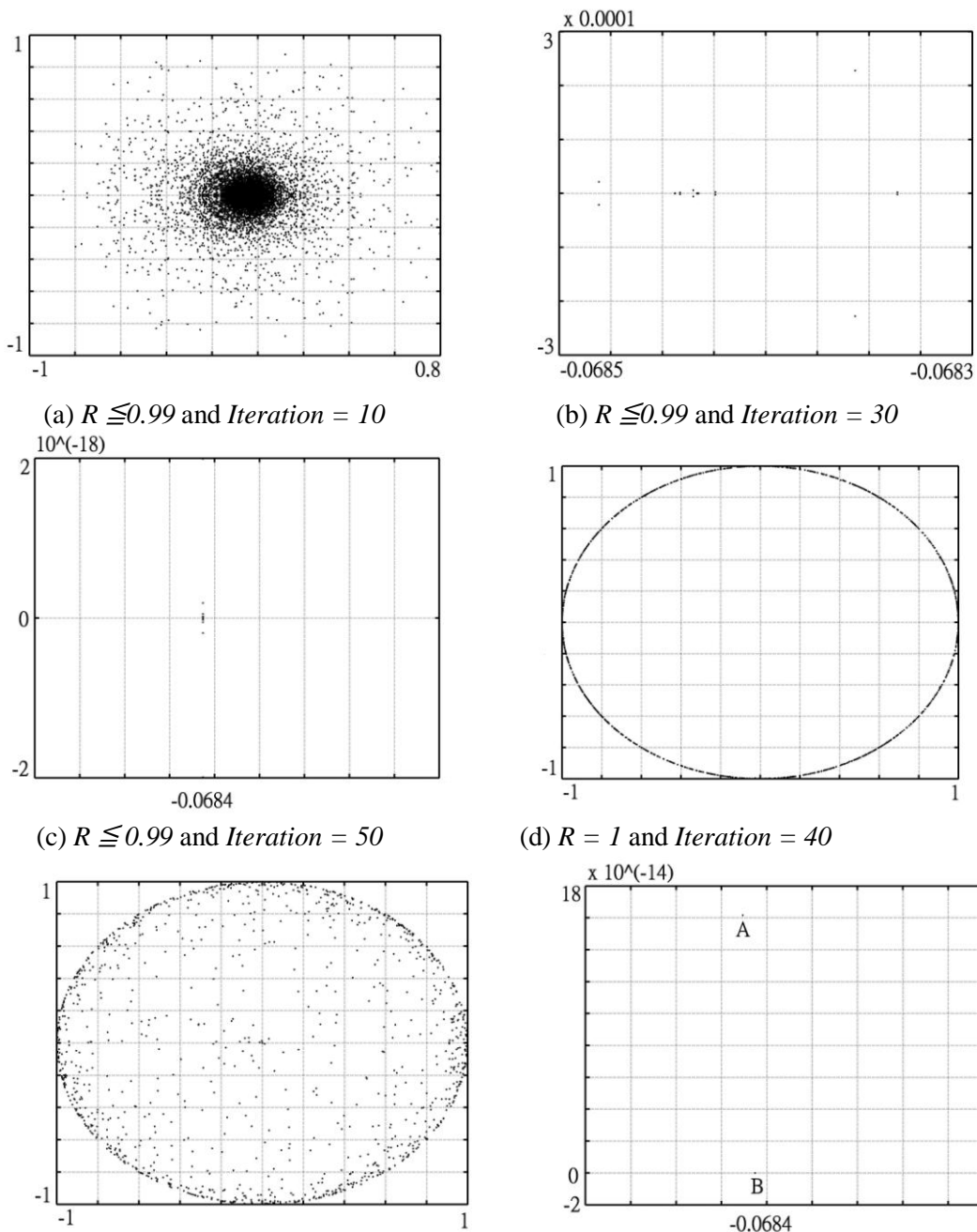
The set of points mapped from the original domain  $(x^2 + y^2)^{1/2} = 1$  does not have real-axis symmetry. The set of points converges to two groups of points (as shown in Fig. 11 (d) through 11(f)). Fig. 11(d) shows all points that are still on the circle wit  $radius = 1$ . Fig. 10(e) shows random distribution. Fig. 11(f) shows two convergent points A and B which are not symmetrical to the real axis. The symmetry broken on the original domains occurs gradually, while the symmetry broken on the mapped domains occurs abruptly.

#### 4.2 Chaos and Compensation

We have illustrated in the section 4.1 (Fig. 10) that when the value of the parameter  $\{a\}$  increases, the original domains become asymmetric to the imaginary axis. We further define this parameter as follows:

$$a = k ( \cos\theta + i*\sin\theta ) \tag{5}$$

Here  $k$  is a constant value. Now we can rotate the original domain on the angle  $\theta$ . Fig. 12 shows that when the bulbs extending from the central portion of the fractal pattern (i.e., Julia sets) have a phase lag against the central portion, the rotation creates symmetry broken as soon as the angle  $\theta$  does not equal to zero. When the rotation angle  $\theta$  increases, bulbs are moving almost to the central regions of two consecutive fractal branches of the central portion. The central portion begins to form ramifications and it is the divergent region (Julia sets) that grows. As the number of iterations increases, a spiral pattern forms connecting bulbs back to the original branches. This connection will prevent the divergent regions from further growing and the fractal pattern will sustain as the iteration increases. When the rotation angle  $\theta$  increases further, the bulbs are connected to the ramifications through spiral patterns (Fig. 12(d) and 12 (e)), the divergence regions grow continuously and eventually the original domain becomes chaotic.



(a)  $R \leq 0.99$  and Iteration = 10

(b)  $R \leq 0.99$  and Iteration = 30

(c)  $R \leq 0.99$  and Iteration = 50

(d)  $R = 1$  and Iteration = 40

(e)  $R = 1$  and Iteration = 40

(f)  $R = 1$  and Iteration = 40

(e)  $R = 1$  and Iteration = 50

(f)  $R = 1$  and Iteration = 100

Figure 11 (a), (b) and (c) are mapped domains with different iterations and symmetry to real axis, 11 (d), (e) and (f) are mapped domains with different iterations and no symmetry to real or imaginary axis. Point set A and B are convergent points

The symmetry broken and chaos formation can be compensated due to domain rotation. The parameter  $\{exp(g_i(z))\}$  plays the key role to offset the phase lag. Fig. 13 shows that when  $g_i(z)$  is designated as a function of angle  $\theta$ , the phase lag is corrected and the entire original domain in fractal patterns rotates in synchronization. By doing so, the symmetry will be maintained and chaos will not occur. Fig. 13(a) shows a phase lag occurring among the central branches and corresponding bulbs as rotation angle is approaching to  $80^\circ$  for the function

$Z^{-1} C_1 C_2 C_3 C_4 C_5$ , which has 4 branches on the central portion. Fig. 13(b) shows the bulbs connected with the ramification branches and chaos occurring at  $\theta = 90^\circ$ . When  $\theta = 100^\circ$ , the bulbs are connected to the neighboring branches and the domain becomes stable once again. With compensation, we can observe that stable domains maintain through different rotation angles as shown at Figure 13 (d) through 13(f).

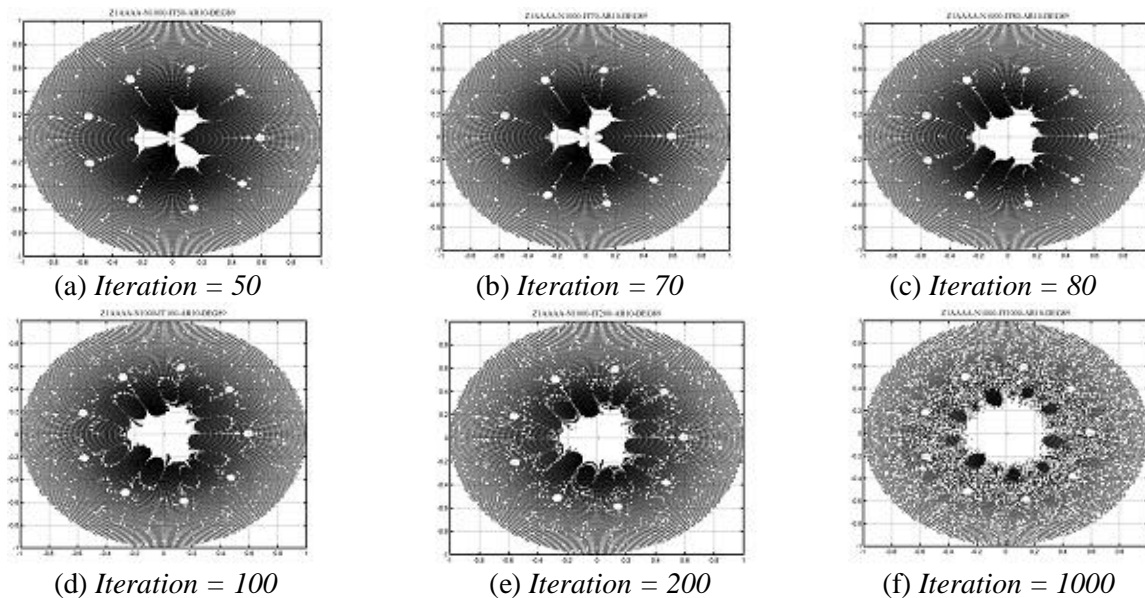


Figure 12 Symmetry broken and Chaos formation induced by domain rotation. 12(a) through (f) shows the divergence of a stable domain

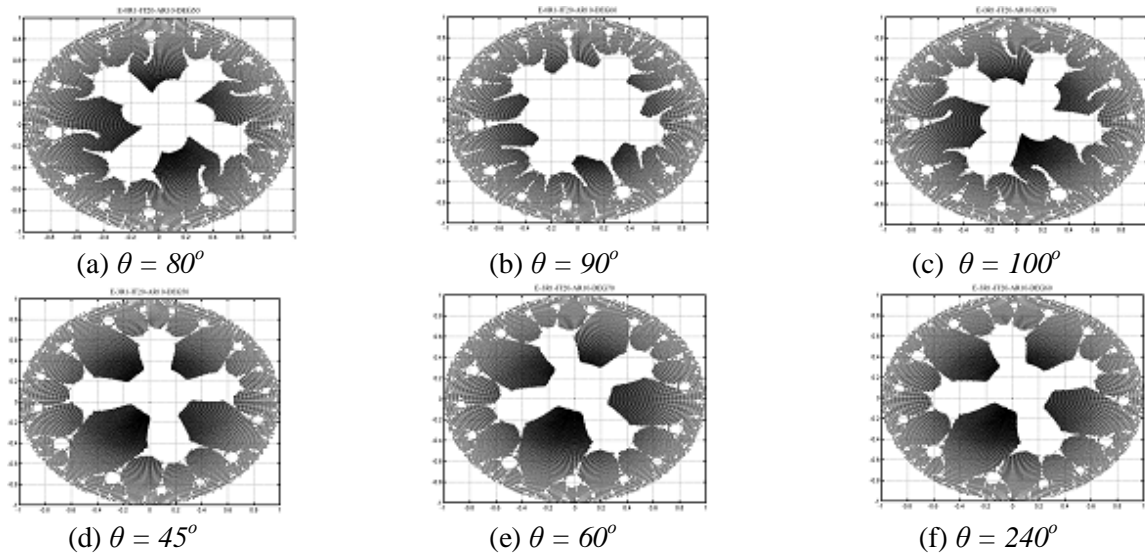


Figure 13 Phase compensation by parameter  $\exp(g_i(z))$  for maintaining symmetrical and stable Herman ring. 13(a) through (c) has no compensation and 13(d) through (f) is compensated.

### 4.3 Fractals and Chaos related to $Z^q$

In the previous sections we selected  $q = -1$  for the term  $z^q$ . We can also examine the original domains when selecting other values. Fig. 14 shows that the original domain becomes chaotic after few iteration with  $a = 0.01$  and  $q = -1.5$  for the function  $Z^{-1}C_1C_2C_3C_4$ . It also shows that extra branches form the central portion (i.e., Julia sets). On the other hand, we select  $q = -0.5$  and  $a = 0.3$  for the original domain (as shown at Fig. 15). In this case, only simple fractals, or Julia sets, are developed and the domains are rather insensitive to the number of parameter subset  $\{a, iteration\}$ .

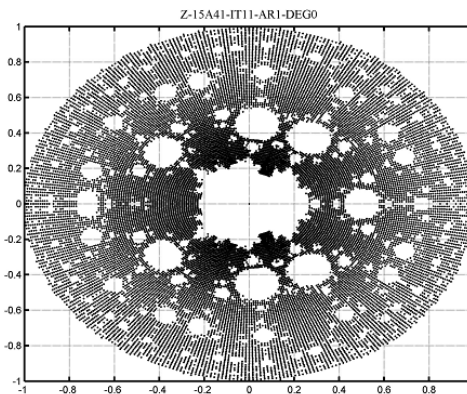


Figure 14 Original domain with  $q = -1.5$ ,  $a = 0.01$ , and  $iteration = 11$

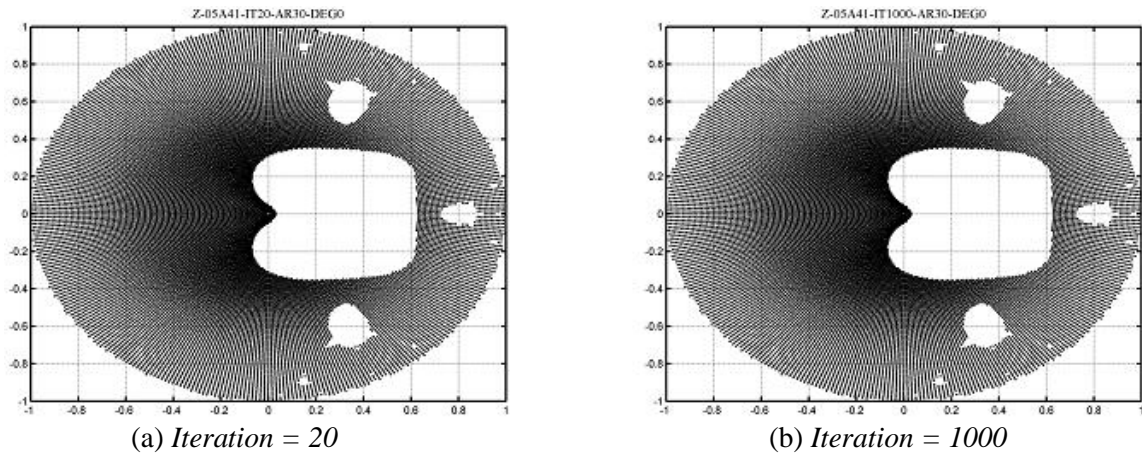


Figure 15 Original domains with  $q = -0.5, a = 0.3$  (a) iteration = 20 (b) iteration = 1000

## 5. Degeneracy

Under certain combinations of the values of the parameters, we have observed that a specific set of original domains show the fractal patterns of the constrained Herman-ring of other classes with different function degrees. We call these types of topological variations as degeneracy.

### 5.1 Phase Degeneracy

For the function of  $Z^{-1} C_1 C_2 C_3$  we add an additional phase item to the formula (5), namely, a phase shift  $\delta_i$  added to  $C_i$  term

$$a_i = k ( \cos(\theta + \delta_i) + i * \sin(\theta + \delta_i) ) \tag{6}$$

Fig. 16(a) shows the normal case and Fig. 16(b) the degenerate one. For each of six branches of the central portion (i.e., Julia sets), there are two bulbs extended toward the boundary of the Herman rings. This figure can be compared with the Herman ring of 8<sup>th</sup> degree (Fig. 6(c)) which shows the six-branch pattern from central portion that extends to the corresponding 6 bulbs.

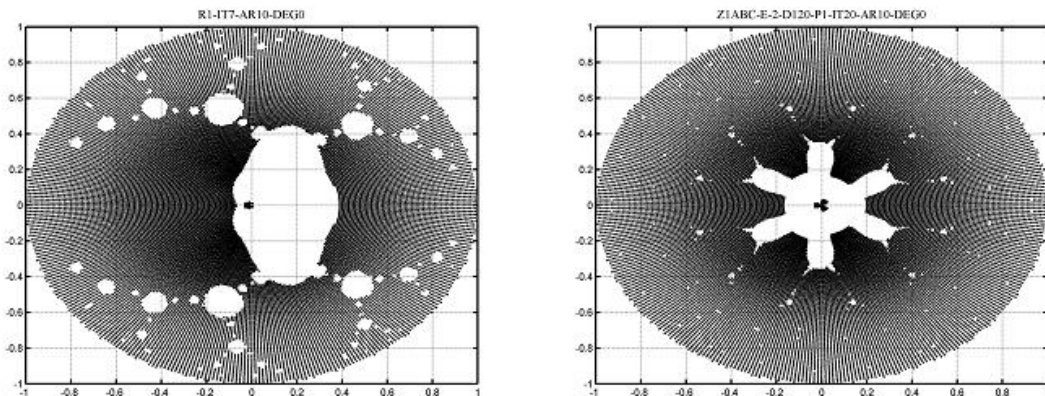


Figure 16 Original domains of the function  $Z^{-1} C_1 C_2 C_3$  (a) normal (b) degenerate

### 5.2 Energy Degeneracy

For the case in section 5.1, the original domain is at scale  $R \sim 10^2$ . Fig. 17 shows a normal case with  $a = 0.01$  and a degenerate case with  $a = 0.99$ . The degenerate domains show the fractal patterns that are similar to the sets of the function  $Z^{-1} C$ . This type of degeneracy is also observed in other high-degree Herman rings, namely,

when the value  $\{a\}$  is approaching to unity, the fractal patterns of high-degree Herman rings transform into the structures that are similar to the patterns of the function  $Z^{-1}C$  (Fig.2).

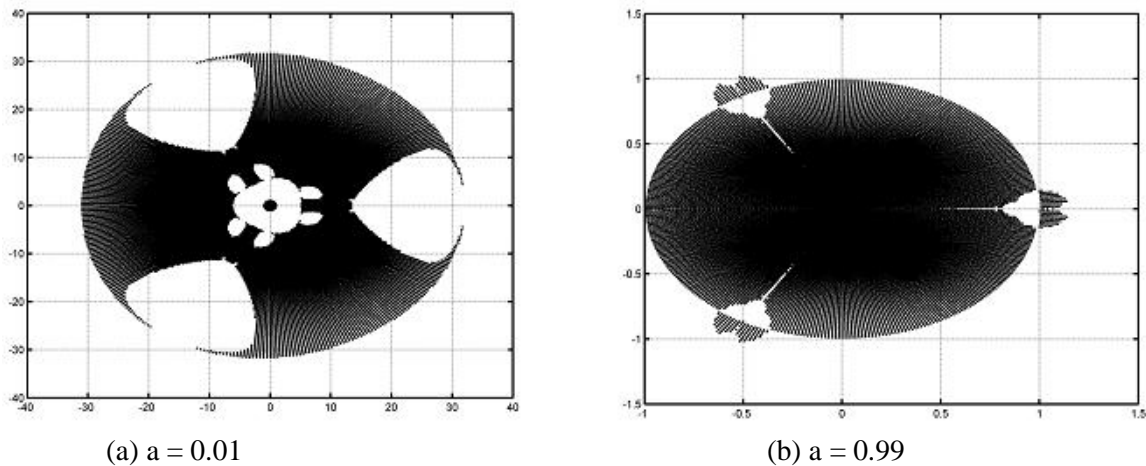


Figure 17 Original domains of the function  $Z^{-1}C_1C_2C_3$  (a)  $a = 0.01$  (b)  $a = 0.99$

## 6. Conclusions

- (1) There are at most five layers of constrained Herman rings at different  $z$  scales with appropriate parameter set. Skip symmetry shows interesting scheme of the rational maps.
- (2) Symmetry broken occurs both in original and mapped domains. The symmetry broken of the mapped domains occurs abruptly at the boundary, while the symmetry broken of the original domains evolves gradually depending on the specific parameters.
- (3) There are several mechanisms inducing chaotic domains in conjunction with parameter space. The chaos induced by domain rotation with parameter  $\{a\}$  can be compensated by the adjusting other parameter  $\{\exp(g_i(z))\}$ .
- (4) The patterns of original domains of a specific degree can be transformed to the patterns of other degrees by manipulating parameter space. A case of degeneracy occurs when the parameter  $\{a\}$  approaches to unity. In this case the domain patterns of high-degree will degenerate to the patterns of the function  $Z^{-1}C$  with  $degree = 2$ .

The richness of these extended Blaschke functions and equations may be valuable to other fields of mathematics and physics. In the future we will continue the exploration of these interesting characteristics in the parameter space and the development their applications to related fields.

## References

- [1] Benoit B. Mandelbrot, "The Fractal Geometry of Nature", New York, W.H. Freeman and Company, 1983.
- [2] J. Milnor, "Dynamics in One Complex Variable", Vieweg, 2000.
- [3] Arnol'd V.I., Small denominators. I: Mappings of the circumference onto itself, Am. Math. Soc., Transl., II. Ser. 46, 213-284 (1965); translation from Izv. Akad. Nauk SSSR, Ser. Mat. 25, 21-86 (1961).
- [4] M. Herman, Uniformit'e de la distortion de Swiatek pour les familles compactes de produits de Blaschke, manuscript, 1987; and the references therein.
- [5] David C. Ni and C. H. Chin,  $Z^{-1}C_1C_2C_3C_4$  System and Application, TIENCS workshop, Singapore, August 1-5, 2006.

- [6] David C. L. Ni and C. H. Chin, *A Novel Approach for Designing Fractal Antennas*, Proc. of International Conference on Wireless Information Networks and Systems, pp. 157-160, (Eds. S.O. Mohammand *et al.*), Barcelona, Spain, July 2007.
- [7] David C. Ni and C. H. Chin, *Broadband Fractal Antennas*, Proc. of International Symposium on Antennas and Propagation, Taipei, Taiwan, pp. 68 (Abstract), October 27-30, 2008.
- [8] C. H. Chin, *Hypertranscendental Geometry*, Preprint NCTU-IMS-0801, Taiwan, R.O.C..
- [9] David C. Ni and C. H. Chin, *Symmetry Broken in Low Dimensional N-body Chaos*, Proc. (CD format) of Chaos 2009 Conference, Chania, Crete, Greece, pp. 53 (Abstract), June 1-5, 2009.
- [10] David C. Ni and C. H. Chin, *Herman Ring Classification on Function*  
 $h(z) \prod_i \{ \exp(g_i(z)) [(a_i - z)/(1 - \bar{a}_i z)] \}$ , Proc. (CD format) of 5th International Conference 2009 - Dynamical Systems and Applications, Constantza, Romania, pp. 48-49 (Abstract), June 15-18, 2009.